LiftWEC

DEVELOPMENT OF A NEW CLASS OF WAVE ENERGY CONVERTER BASED ON HYDRODYNAMIC LIFT FORCES

Deliverable D6.1

Extreme Event LiftWEC ULS Assessment

Deliverable Lead	University of Strathclyde
Delivery Date	30th November 2020
Dissemination Level	Public
Status	Final
Version	**1.3**

This project has received funding from the European Union's Horizon 2020 research and innovation programme under grant agreement No 851885. This output reflects the views only of the author(s), and the European Union cannot be held responsible for any use which may be made of the information contained therein.

Document Information

Project Acronym	LiftWEC
Project Title	Development of a new class of wave energy converter based on hydrodynamic lift forces
Grant Agreement Number	851885
Work Package	WP6
Related Task(s)	T6.1
Deliverable Number	D6.1
Deliverable Name	Extreme Event LiftWEC ULS Assessment
Due Date	30th November 2020
Date Delivered	30th November 2020
Primary Author(s)	Abel Arredondo Galeana (UoS)
Co-Author(s)	Weichao Shi (UoS), Feargal Brennan (UoS)
Document Number	LW-D06-01

Version Control

Revision	Date	Description	Prepared By	Checked By
1.0	6/10/2020	Internal working draft	AAG	WS, FB
1.1	6/11/2020	Internal draft for review	AAG	WS, FB
1.2	10/11/2020	Draft for consortium Review	AAG	WS, FB
1.3	30/11/2020	Submission to EU	AAG	WS, FB

This project has received funding from the European Union's Horizon 2020 research and innovation programme under grant agreement No 851885. This output reflects the views only of the author(s), and the European Union cannot be held responsible for any use which may be made of the information contained therein.

EXECUTIVE SUMMARY

This document constitutes Deliverable '*D6.1 Extreme Event LiftWEC ULS Assessment"* of the LiftWEC project. LiftWEC is a collaborative research project funded by the European Union's Horizon 2020 Research and Innovation Programme under Grant Agreement No 851885. It is the intention of the project consortium that the LiftWEC project culminates in the development of one or more promising configurations of a Wave Energy Converter operating through the use of one or more rotating hydrofoils that generate lift as the primary interaction with the incident waves.

In this report, a structural analysis methodology is developed to ensure the survivability of LiftWEC under extreme operating conditions. For a wave cyclorotor or the LiftWEC concept, extreme operating conditions are considered as the primary design conditions in a similar manner to the Atargis system's approach [Siegel, 2019]. This is because first, the maximum lift force in LiftWEC occurs in operating conditions, and secondly, because it operates in a submerged manner, hence slamming and wave-impact loads are avoided.

At this stage, seventeen concept designs were developed within the consortium. As such, this report presents an introductory classification of the major commonalities. Subsequently, two representative configurations are selected to perform the structural analysis. In the first configuration, the hydrofoils are supported at both ends, and in the second configurations, the hydrofoils are supported only in the middle. A bottom-fixed frame is assumed as the support structure for both configurations.

Given that the purpose of this report is to detail the Ultimate Limit State (ULS) methodology, "typical" loading and material strength properties are applied here for illustrative purposes. Wave operating conditions are selected from literature and we compare these conditions to wave data from a point in the Atlantic coast of France. A moderate strength offshore structural steel is selected as the construction material, and the structural integrity of the device is assessed subject to hydrodynamic loading derived from irregular waves.

It is worthy to note that a limit state is a condition beyond which a structure or a part of a structure exceeds a specified design requirement. For example, ULS can be defined as a condition where a loss of structural resistance occurs. Additionally, partial safety factors can be considered to account for abnormal operating conditions. As such, here we defined the threshold for the ULS as one third of the yield stress level. This threshold however can be refined to meet future design specifications.

The structural analysis is carried out on three substructures: the hydrofoils, the attachment structures between rotor and hydrofoils and the support structure. Python, Abaqus and SkyCiv are utilised to perform and validate the structural analysis. Shear forces, bending moments and deflections are computed, and maximum stresses are computed in the substructures. It is found that in LiftWEC, the substructures that undergo the highest bending stresses are the hydrofoils. However, for the conditions examined, the stress levels remain below the allowable stress level for a wide range of hydrofoil spans.

This project has received funding from the European Union's Horizon 2020 research and innovation programme under grant agreement No 851885. This output reflects the views only of the author(s), and the European Union cannot be held responsible for any use which may be made of the information contained therein.

TABLE OF CONTENTS

This project has received funding from the European Union's Horizon 2020 research and innovation programme under grant agreement No 851885. This output reflects the views only of the author(s), and the European Union cannot be held responsible for any use which may be made of the information contained therein.

1 INTRODUCTION

Wave Energy has enormous potential, however the aggressive manner in which wave loads are imparted into conventional WECs means that often WEC materials and structures struggle to resist cyclic and variable impact environmental loads resulting in very large costs and poor structural reliability. LiftWEC by its definition harnesses wave forces in a constant and even manner which in addition to allowing better control for optimum power take-off means that loads imparted to the WEC structure will be less aggressive.

This deliverable is focused in developing a structural assessment methodology to ensure that LiftWEC can be operated in a structurally reliable manner. Seventeen concept configurations of LiftWEC are studied and their major commonalities are identified. Two sample configurations are down selected to carry out the structural analysis. This is achieved through analytical methods supported with two-dimensional finite element analysis.

Given that the purpose of this report is to detail the Ultimate Limit State (ULS) methodology, "typical" loading and material strength properties are applied here for illustrative purposes. An irregular sea state is utilised to compute angles of attack and inflow velocity time series' for each LiftWEC hydrofoil. Loading distributions along the hydrofoils are then calculated using these timeseries inputs. The maximum values of the time series are chosen as the extreme test case for the LiftWEC structure. It is noted that the maximum loads that LiftWEC can experience in an irregular sea state can be between 3 to 4 times higher than in a regular sea state. As such, it is important to consider an irregular sea state for the structural analysis. It is also important to note, that extreme loads in a cyclorotor, such as LiftWEC, occur during operating conditions (Siegel, 2019). This is because lift generation stops once the stall angle is exceeded and because LiftWEC operates in a submerged manner, preventing slamming loads from being an issue.

1.1 PURPOSE OF DELIVERABLE

The purpose of this deliverable is to provide guidelines for the safe structural design of the LiftWEC rotor. This is performed by computing the loads on the hydrofoils and propagating the loads through the rest of the structure. The study is mostly performed by means of beam theory and frame analysis, supported in some cases by two-dimensional finite element analysis. Shear forces, bending moments and deflections are computed. Maximum stresses are compared to the allowable stress level and guidelines are provided to size LiftWEC in a structural compliant fashion.

1.2 STRUCTURE OF THE DOCUMENT

The structure of this report is as follows. First, an introduction to the background studies is provided. Secondly, several LiftWEC configurations proposed in the Lisbon workshop are studied and their commonalities are identified. The commonalities are grouped under three different categories: 1) Components, 2) Type of support structure and 3) Type of Power take-off (PTO). This classification is used to select two representative configurations for the structural analysis.

This project has received funding from the European Union's Horizon 2020 research and innovation programme under grant agreement No 851885. This output reflects the views only of the author(s), and the European Union cannot be held responsible for any use which may be made of the information contained therein.

Subsequently, the wave operating conditions are selected, and the hydrodynamic model is introduced. The structural analysis is carried out on three components: 1) hydrofoils, 2) attachment pieces between hydrofoils and rotor and 3) support structure. Shear forces, bending moments and deflections are computed. Maximum bending stresses are quantified on the substructures and results are analysed. Finally, the relevant conclusions are presented.

1.3 BACKGROUND STUDIES

Little has been reported on the structural modelling of LiftWEC-like rotors. The most comprehensive structural study has been reported by Siegel, 2019. In his study, Siegel provides a schematic of a two-hydrofoil rotor that operates in water depths of 40 m and that is submerged by 12 m. The rotor has a diameter of 12 m and the chord length of the hydrofoils is 5 m. The hydrofoils have a span of 60m and are supported end to end. The material used is standard carbon steel. The support structure is a bottom fixed frame and the attachment legs are grounded 60 m apart. This is shown in figure 1.

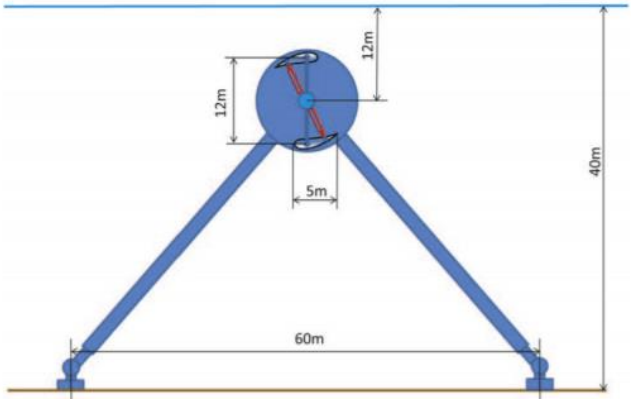

Figure 1. CycWEC rotor from Siegel, 2019 [1].

In Siegels' work, all structural loads were estimated based on hydrofoil lift and drag coefficients published by Sheldahl & Klimas, 1983. For a given sea state, the relative hydrofoil flow velocity is found as the vectorial sum of the rotational velocity of the hydrofoil and the wave induced velocity. The latter is estimated using Airy wave theory (Airy, 1845). The load at each spanwise location is determined assuming an elliptical spanwise lift distribution. The total lift force is integrated over the span of the hydrofoils. The sea states used in Siegel's work are listed in Table 1.2. He considers three sea states: design, storm and shortest.

Table 2
CycWEC design sea states.

Wave	Height [m]	Period [s]
Design	2.25	10.5
Storm	15	15
Shortest	1.75	6

Table 1. Test case conditions adapted from Siegel, (2019).

This project has received funding from the European Union's Horizon 2020 research and innovation programme under grant agreement No 851885. This output reflects the views only of the author(s), and the European Union cannot be held responsible for any use which may be made of the information contained therein.

He finds that the loads experienced in storm do not exceed the ones in operational mode. This is because the rotational speed of the rotor is inversely proportional to the period of the incoming wave, and since the wave period for the storm sea state is much larger than in the operational sea state, the rotational velocity and the loads in storm are smaller. It is also noted that although Siegel states that accurate structural loads can be obtained, by using simple hand calculations to propagate design loads from the hydrofoils through the structure, his methodology is not explicit. Another limitation in his work is that for large spans, hydrofoils would tend to experience two-dimensional flow and therefore uniform loading, rather than elliptical loading. Hence his observations could be underestimating the actual loads on the hydrofoils and the structure.

2 CLASSIFICATION OF PROTOTYPES

2.1 INTRODUCTION

Seventeen candidate concept designs were presented during the online Lisbon workshop in May 2020. An example configuration is observed in Figure 2. The structure comprises (1) two hydrofoils, (2) the attachment pieces between the hydrofoil and the rotor, (3) the support structure and (4) the hub or rotor. In the figure, F, A and M are the normal and axial forces, and the pitching moment acting on the hydrofoils. While, F_{rz}, F_{rx} and T are the normal and axial forces, and the torque on the rotor.

The main characteristics of the seventeen LiftWEC concepts were grouped into three categories: 1) structural components, 2) type of support structure and 3) type of power take-off. The classification branches are explored with three diagrams in the following sections, while a summary table of the structural characteristics of the seventeen prototypes is presented in Appendix 1.

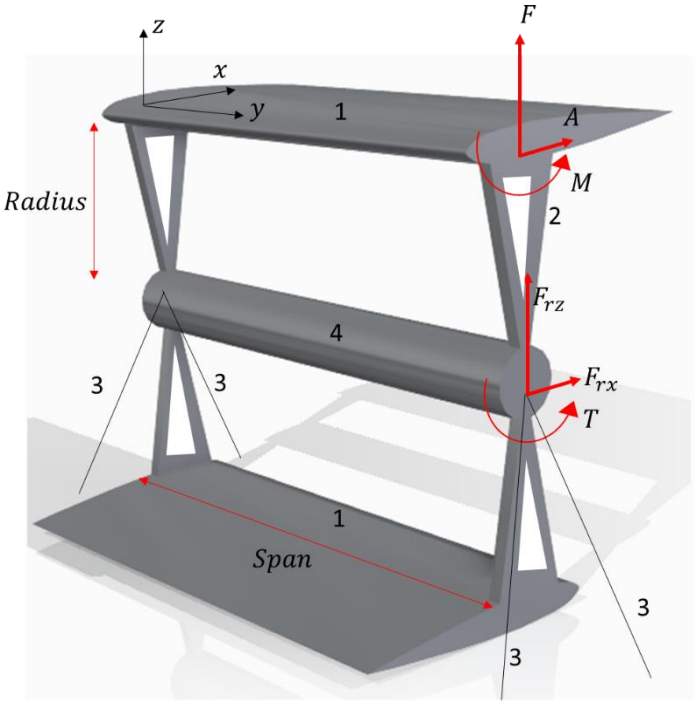

Figure 2. CAD rendering of a LiftWEC device.

This project has received funding from the European Union's Horizon 2020 research and innovation programme under grant agreement No 851885. This output reflects the views only of the author(s), and the European Union cannot be held responsible for any use which may be made of the information contained therein.

2.2 STRUCTURAL COMPONENTS

This subsection classifies the LiftWEC configurations in terms of their main structural components.

LiftWEC configurations may or may not include a central hub. With a central hub, the hydrofoils are connected to the hub and drive its rotation. For example, see the device shown in Figure 2. The hub is typically connected to a power take-off (PTO) mechanism. In contrast, hubless devices drive the PTO by directly coupling the motion of the hydrofoils to the PTO. This means that the hydrofoils are directly connected with some structure to the PTO.

The support structures for the hydrofoils for hub and hubless devices, are typically spokes or discs. In the case of a hub, these support structures emerge from the hub and expand towards the hydrofoils. The spokes or discs can be at both ends of the hub or located only in the middle. For a hubless device, the support structures for the hydrofoils are not connected to a central hub, but instead to a rotational mechanism (bearing or PTO) at each end of the LiftWEC device.

All combinations can exist in a two-hydrofoil or in a multifoil configuration. A summary of these combinations is shown in the tree diagram of Figure 3.

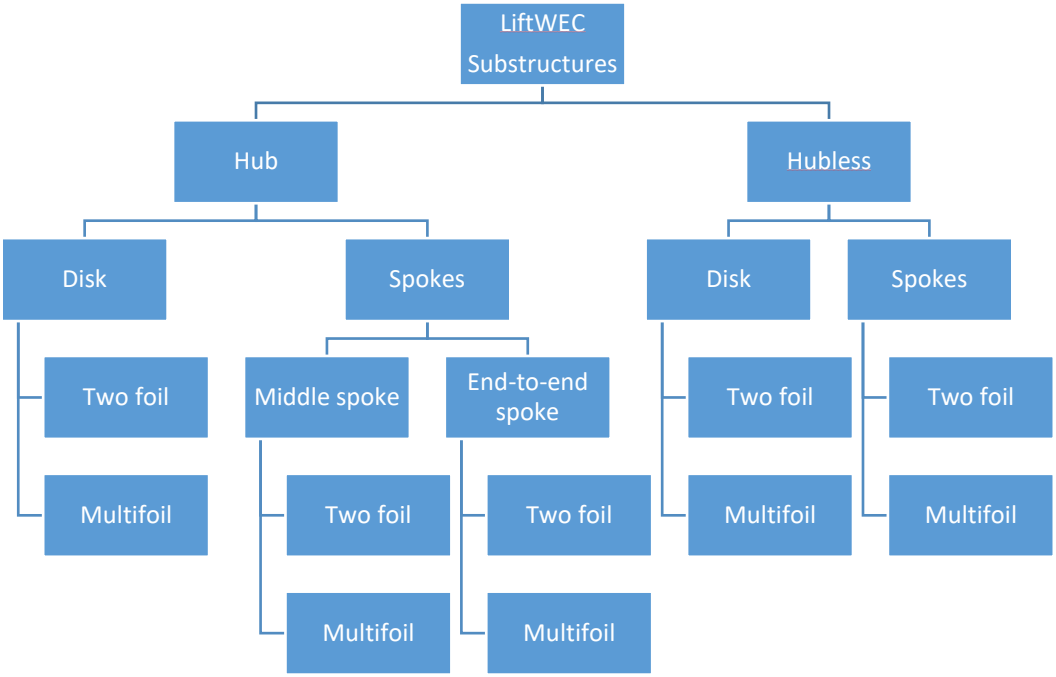

Figure 3. LiftWEC classification due to substructures.

This project has received funding from the European Union's Horizon 2020 research and innovation programme under grant agreement No 851885. This output reflects the views only of the author(s), and the European Union cannot be held responsible for any use which may be made of the information contained therein.

2.3 SUPPORT STRUCTURE

The support structures can be classified into 1) floating, 2) slack or taut mooring lines, 3) jack-up struts or 4) monopiles. The choice of the support structure will depend on the reaction source of the device, the water depth, and the cost of the support structure. Figure 4 shows a tree diagram of the possible support structures.

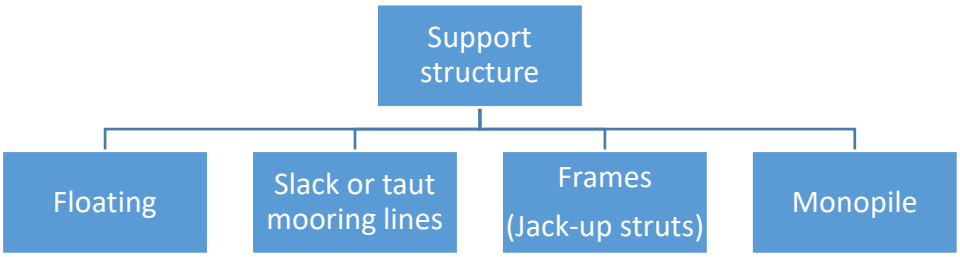

Figure 4. LiftWEC classification due to type of support structure.

2.4 POWER TAKE-OFF LOCATION

Two types of power take-off (PTO) mechanisms were identified. One where the PTO is centrally located and driven by the torque generated by the axial force of the rotating hydrofoils; and another one where the PTO is mounted as an independent unit on top of the hydrofoils. This latter configuration can be found for example in the Minesto device. A description of this latter type of PTO can be found at: https://minesto.com/our-technology. Figure 5 shows a tree diagram with the two types of PTO.

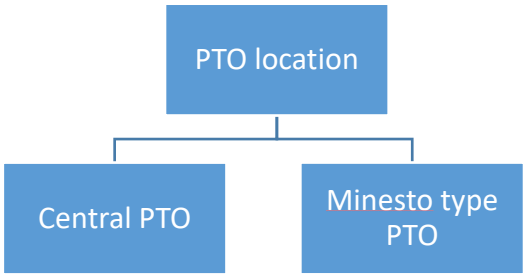

Figure 5. LiftWEC classification due to location of power take off (PTO).

This project has received funding from the European Union's Horizon 2020 research and innovation programme under grant agreement No 851885. This output reflects the views only of the author(s), and the European Union cannot be held responsible for any use which may be made of the information contained therein.

3 WAVE CONDITIONS

According to the Grant Agreement No 851885, the basis of design is associated with the large-scale production of energy for the European market using the North Atlantic wave climate. As an example, we analyse wave data from the Atlantic coast of France. Sierra et al. (2017) showed that most of the energy there is concentrated in sea states with an energy period (T_e) between 10 and 12 s and significant wave height (H_s) between 2 and 4 m. For LiftWEC, we consider a Jonswap wave spectrum with a peak wave period (T_p) of 10 s and a significant wave height (H_s) of 4 m.

We put our testing wave conditions into context in figure 6. The figure shows a scattered plot of the Homere database with T_e along the horizontal axis and H_s along the vertical axis. The scatter plot corresponds to a point in the North Atlantic at the coast of France, located at 47.84° N, 4.83° W. The red marker in the figure shows our testing conditions ($T_p = 10$ s, $H_s = 4$ m). The conversion from T_p to T_e is performed through $T_e = \alpha T_p$, where $\alpha = 0.9$ for a Jonswap wave spectrum (Cornet 2008).

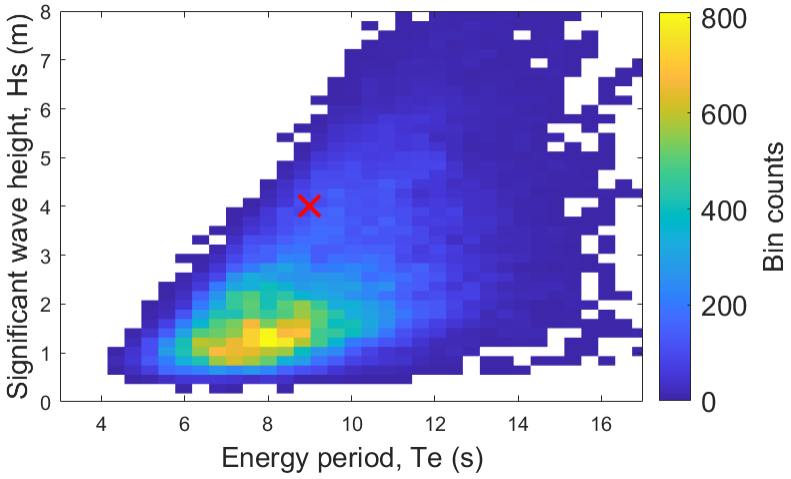

Figure 6. Energy period (T_e) versus significant wave height (H_s) from Homere database, for a location from the North Atlantic coast of France close to Quimper at 47.84° N, 4.83° W.

We compare our design testing conditions to those of Siegel (2019) in table 2. The testing conditions for Siegel's cyclorotor device are selected from the US west coast at Humboldt Bay. We observe that H_s in Siegel's work is about half to that tested here, while T_p is similar. In the next section, we show that forces on LiftWEC are more sensitive to rotational velocities, and so testing with similar periods means that both devices will operate within a range of similar forces.

	Condition	T_p (s)	H_s (m)
Siegel, 2019	Design	10.5	2.25
LiftWEC (Deliverable D6.1)	Design	10.0	4.00

Table 2. Peak period (T_p) and significant wave height (H_s) for design conditions tested in Siegel 2019 and for LiftWEC (Deliverable D6.1).

This project has received funding from the European Union's Horizon 2020 research and innovation programme under grant agreement No 851885. This output reflects the views only of the author(s), and the European Union cannot be held responsible for any use which may be made of the information contained therein.

4 LOADS ON HYDROFOILS

The lift and drag forces for a two-hydrofoil system are computed with the hydrodynamic code provided by consortium partner Hamburg University of Technology (TUHH).

The code utilises a NACA 0012 profile for each hydrofoil. The two dimensional lift and drag coefficients (C_L, C_D) curves of the profile are taken from Sheldahl & Klimas (1981) at a Reynolds number (Re) of $10 \times 10^6$and plotted in figure 7. We expect two-dimensional flow due to large-spanned hydrofoils, whereas for short-spanned hydrofoils, two-dimensionality can be promoted through winglets or splitter plates at each end of the hydrofoils.

It can be seen in figure 7 that the maximum C_L is reached at an angle of attack of about $\alpha = 14^{\circ}$. Contrarily, maximum C_D occurs at $\alpha = 90^{\circ}$, i.e. when the hydrofoil is normal to the incoming flow.

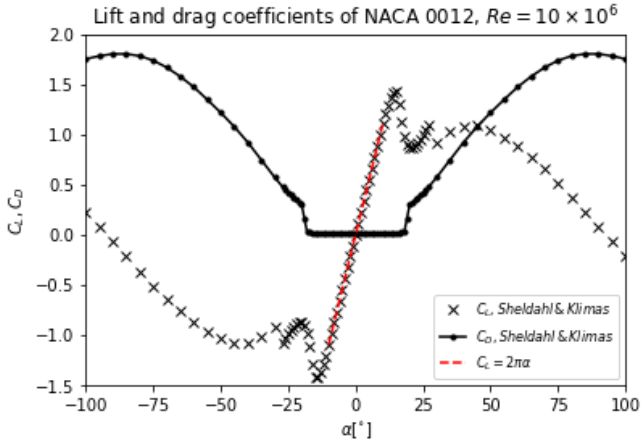

Figure 7. Lift and drag coefficients (C_L, C_D) for a NACA 0012 at $Re = 10 \times 10^6$ in a range of angles of attack (α) between-100 to 100 degrees.

The lift and drag forces on the hydrofoils are computed with

$$L = \frac{1}{2}\rho w^2 b c C_L \qquad 4.1$$

and

$$D = \frac{1}{2}\rho w^2 b c C_D, \qquad 4.2$$

where ρ is the fluid density, w is the relative velocity of the incoming flow, b is the span of the hydrofoil, c is the chord length and C_L and C_D are the lift and drag force coefficients from figure 7.

To quantify the forces on the hydrofoils, consider figure 8a. The figure shows a LiftWEC rotor with two hydrofoils. In the figure, u is the velocity due to the motion of the hydrofoil, v is the wave velocity, w is the relative velocity, L is the lift force and D is the drag force. The velocity due to the motion of the hydrofoil is the opposite of the hydrofoil rotational velocity, such that

$$u = -\omega r, \qquad 4.3$$

This project has received funding from the European Union's Horizon 2020 research and innovation programme under grant agreement No 851885. This output reflects the views only of the author(s), and the European Union cannot be held responsible for any use which may be made of the information contained therein.

where ω is the angular velocity of the rotor and r is the rotor radius. Here we set ω to a fixed value and equal to $\omega = 2\pi/T_p$. The wave velocity v is computed from Airy linear wave theory (Airy 1845). We can compute $\boldsymbol{w}$ from the vectorial sum of $\boldsymbol{u}$ and $\boldsymbol{v}$, such that

$$\boldsymbol{w} = \boldsymbol{u} + \boldsymbol{v} \quad 4.4$$

and the magnitude of $\boldsymbol{w}$ is given by

$$w = \sqrt{u^2 + v^2}. \quad 4.5$$

The angle of attack is determined by computing the cross product of w and u, and dividing it by the product of their Euclidian norm, such that

$$\alpha = arcsin\left[\frac{w \times u}{\|w\|\|u\|}\right]. \quad 4.6$$

Once α is known, C_L and C_D are obtained from figure 7 and the forces L and D can be computed with equations 4.1 and 4.2.

For the case of a regular sea state, figure 8b shows the time evolution of w, α, C_L, C_D, L and D for the two hydrofoils, for a time interval of 60 seconds. The simulation parameters for these time series are $T_p = 10$ s, $H_s = 4$ m, $b = 6$ m, $c = 1$ m, rotor diameter (Ø) of 1 m, a submergence (sd) of -3 m and a phase angle of 90 degrees with respect to the phase of the incoming wave (i.e. phase-locked). From figure 8b, the maximum lift force occurs in hydrofoil 2 and is approximately 2,500 N. We note that with a phase of negative 90 degrees the maximum lift force occurs in hydrofoil 1. For shorter T_p, the load on the hydrofoil increases. This is because ω is inversely proportional to T_p. This was noted by Siegel, 2019 in his latest manuscript, where he noticed that shorter wave conditions typically incur in higher loads.

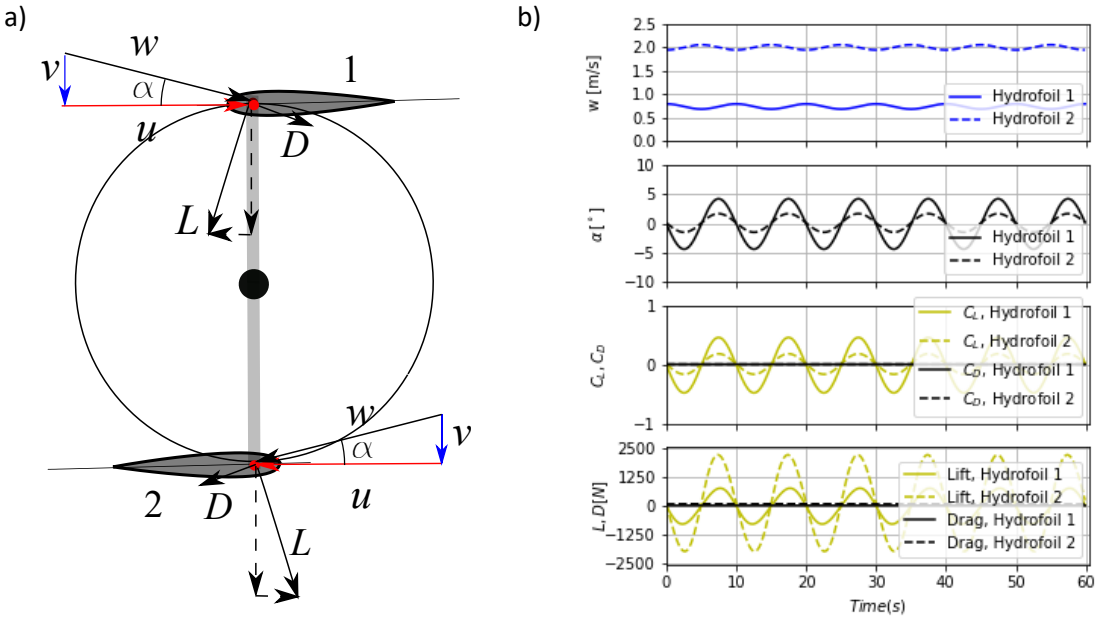

Figure 8. a) Forces on hydrofoils for a two-hydrofoil LiftWEC rotor and b) time series of relative velocity (w), angle of attack (α), lift and drag coefficients (C_L, C_D) and lift and drag forces on two hydrofoils (L, D).

This project has received funding from the European Union's Horizon 2020 research and innovation programme under grant agreement No 851885. This output reflects the views only of the author(s), and the European Union cannot be held responsible for any use which may be made of the information contained therein.

For an irregular sea state, the wave induced velocity v can be computed by discretising a wave energy spectrum to generate individual wave components that can be added up (Siegel, 2019; Jeans et al, 2013). We discretise the above mentioned Jonswap wave energy spectrum and test it to a significant duration (>100Tp) to identify the extreme loads. The hydrodynamic code outputs for irregular waves is shown in Figure 9, for the same simulation parameters as those used in figure 8b. In figure 9, w and α for hydrofoil 1 and hydrofoil 2 are shown in the first two rows, and for clarity only C_L, C_D, L and D of hydrofoil 1 are plotted in the last two rows. The highest lift force is about 8,500 N. In this instance and after 120 T_p, it is observed that an irregular sea state could multiply the regular wave loading by a factor of 3 to 4.

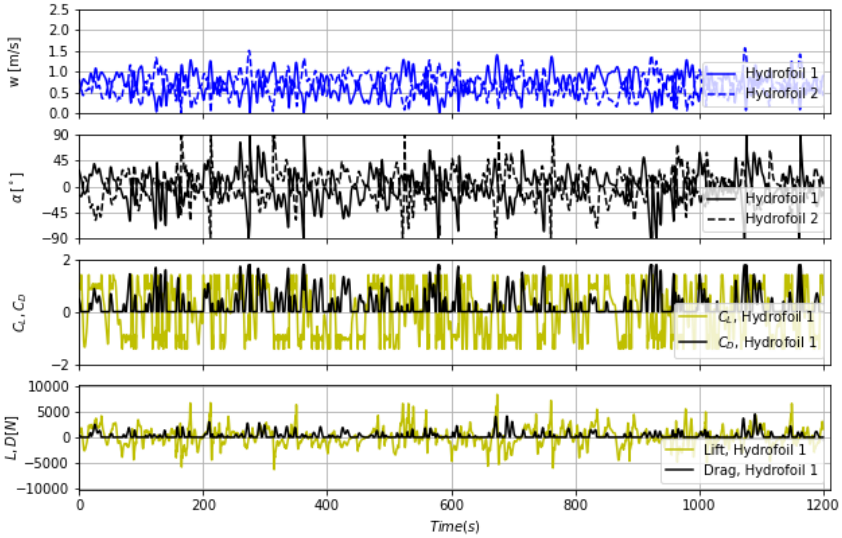

Figure 9. Time series of the angle of attack (α), relative velocity (w) for hydrofoil 1 and hydrofoil 2,and lift and drag coefficients (C_L, C_D), lift and drag forces (L, D) for hydrofoil 1.

The size of the hydrofoil also affects the generated forces, as indicated by equations 4.2 and 4.3. This means that the lift force will change depending on b and c. From figure 9, we take the maximum C_L ($C_L = 1.42$) and maximum w ($w = 1.4$ m/s) for hydrofoil 1 and recompute the lift force on the hydrofoil. We vary b from 0 to 60 meters and c from 1 to 4 meters. The latter is increased with discrete steps of 1 meter. Results are plotted in figure 10. A maximum expected lift force of 23 kN is reported by Siegel (Siegel, 2012) in the Atargis Final Scientific report for a rotor of $s = 4.5$ m and $c = 0.75$ m, tested at T_p=2.5 s. The forces of figure 10 are for a range of values of T_p= 10 s, hence for the dimensions tested by Siegel, the forces in the figure are expected to be smaller.

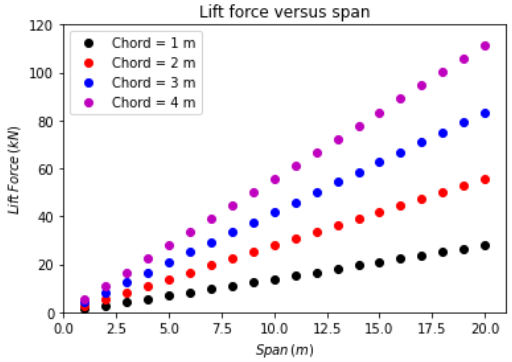

Figure 10. Lift force dependency on span (b) and chord length (c) at $C_L = 1.42$, $w = 1.4\ m/s$, $\rho = 1000\ kg/m^3$.

This project has received funding from the European Union's Horizon 2020 research and innovation programme under grant agreement No 851885. This output reflects the views only of the author(s), and the European Union cannot be held responsible for any use which may be made of the information contained therein.

5 STRUCTURAL ANALYSIS

5.1 CONFIGURATIONS

Two configurations are selected for this study. One where the hydrofoils are supported at each end (Figure 12a) and one where the hydrofoils are centrally supported (Figure 12b). We refer to these configurations as the fixed beam and the cantilever beam configurations, respectively. These arrangements are selected because they represent the layout of most of the configurations identified in Lisbon workshop.

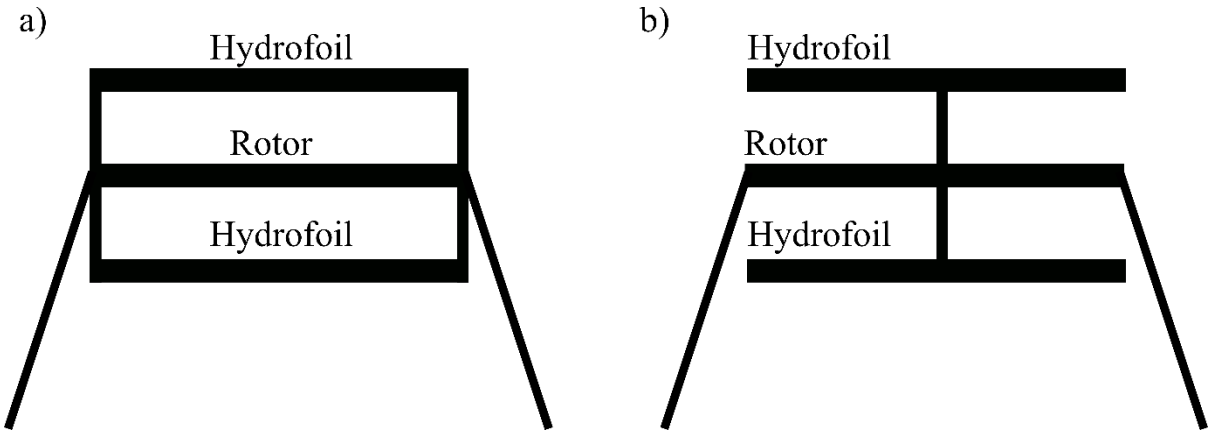

Figure 12 a) LiftWEC rotor with hydrofoils supported at both ends and b) LiftWEC rotor with hydrofoils supported in the middle and with free ends.

5.2 STRUCTURAL SPECIFICATIONS

A moderate strength steel used for offshore applications (Billingham, et al. 2003) is selected as the construction material. Steel is listed as one of the materials towards certification by DNV GL, according to guideline *DNVGL-SE-0120 Certification of Wave Energy Converters and Arrays*. The mechanical properties of the selected steel are listed in table 3.

Material	Steel for offshore applications
Yield stress (σ_{yd})	350 MPa
Ultimate strength (σ_{ul})	410 MPa
Allowable stress ($0.33\sigma_{yd}$)	115.5 MPa

Table 3. Mechanical properties of moderate strength offshore steel: yield stress (σ_{yd}), ultimate stress (σ_{ul}) and allowable stress $(0.33\sigma_{yd})$.

In the table, the allowable stress level is defined as one third of the yield stress level (σ_{yd}). This is the threshold recommended on this deliverable to ensure a structural reliable operation and provide a safety factor for the structure. However, different thresholds can be selected according to design specifications. Lift and drag forces are considered in the rest of the structural analysis.

This project has received funding from the European Union's Horizon 2020 research and innovation programme under grant agreement No 851885. This output reflects the views only of the author(s), and the European Union cannot be held responsible for any use which may be made of the information contained therein.

5.2.1 Hydrofoil cross-section

The hydrofoil is modelled as a single beam of uniform cross-section. The cross-section is a hollow square and is centred at a one-quarter distance from the leading edge of the foil. Assuming a NACA 0012 profile of chord length c, the cross-section has a length of $0.12c$. The neutral axis is aligned with the chord of the foil, as shown in figure 11.

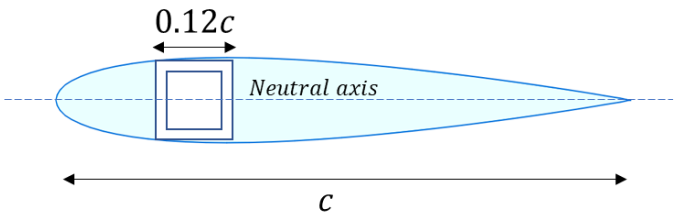

Figure 11. Hollow-square cross-section utilised in structural analysis for NACA 0012 hydrofoil.

Four chord lengths are selected for the study and the corresponding cross section properties (length, height, thickness and second moment of areas) are specified in table 4.

Chord length (m)	Length (m)	Height (m)	Thickness (mm)	Second moment of area (mm^2)
1	0.12	0.12	12.5	9 820 000
2	0.24	0.24	16.0	133 000 000
3	0.36	0.36	16.0	389 000 000
4	0.30	0.48	16.0	818 000 000

Table 4. Chord lengths and properties of cross sections (length, height, thickness, second moment of area) utilised on this study.

The cross sections were sized according to commercially available parts found on the Interactive Steel for life Blue Book website (https://www.steelforlifebluebook.co.uk/).

5.2.2 Flexural formula

The maximum fibre stress in the cross section occurs at the most distant point from the neutral axis (Young and Budynas 2002) and is given by

$$\sigma_{max} = \frac{M_{max} z_{max}}{I} \qquad 5.1$$

where M_{max} is the maximum bending moment, z_{max} is the maximum distance from the neutral axis to the outermost point of the beam and I is the second moment of area of the cross section. Due to the location of the neutral axis in figure 11, in our study, $z_{max} = 0.06c$.

5.2.3 Load distribution on hydrofoils

The typical load distribution over an elliptic finite aspect ratio wing was discovered by Prandtl (Prandtl 1923) and is shown in figure 12a. In such type of wing, the downwash of the tip vortices reduces the

This project has received funding from the European Union's Horizon 2020 research and innovation programme under grant agreement No 851885. This output reflects the views only of the author(s), and the European Union cannot be held responsible for any use which may be made of the information contained therein.

loading towards the tips of the wing. Contrarily, for a LiftWEC device of infinite or very large span, we expect two-dimensional flow and uniform loading. This is depicted as the solid boundary of figure 12b. In the figure, we also plot elliptical (dotted line), quadratic (starred line) and linear (dashed-dotted line) loading distributions. This illustrates what could be potential role of three-dimensional effects on the loading of the hydrofoil.

We utilise the uniform loading and the linear loading as two extreme cases to compute the shear forces, bending moments and deflections over hydrofoils of different span. The uniform loading is the loading distribution due to two-dimensional flow, where no three-dimensional effects are present (tip vortices, spanwise flow, etc). For studies on low aspect ratio wings, see for example DeVoria and Mohseni (2017), where the tip vortices approach the centre of the wing and a linear-type of loading could be present.

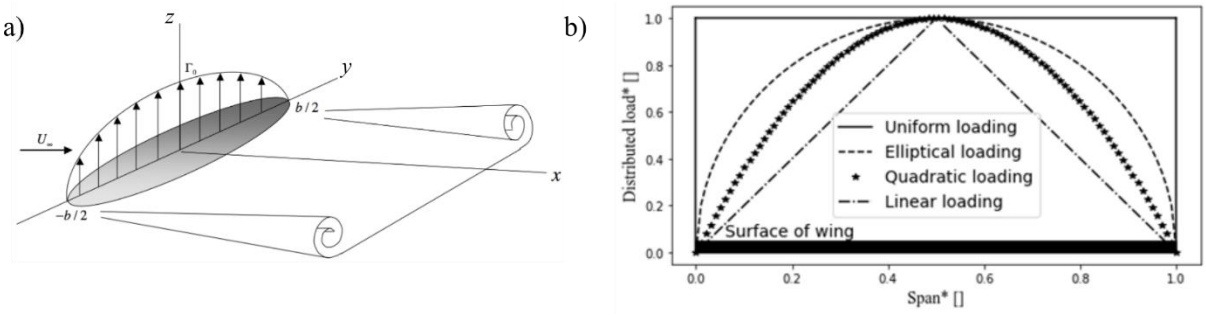

Figure 12 a) Elliptic lift distribution on elliptical finite aspect ratio wing from Chapter 12 Wings of finite span by Cantwell, where b is the span and U_∞ is the freestream velocity and b) different types of loading on the surface a wing: uniform, elliptical, quadratic and linear.

5.3 STRUCTURAL ANALYSIS OF HYDROFOILS

Consider the hydrofoils of LiftWEC as beam structures. Figure 13a shows a fixed beam support at both ends, which corresponds to the full length of the hydrofoil in the fixed beam configuration. Figure 13b shows a cantilever beam supported at one end, which corresponds to half the full length of the hydrofoil in the cantilever beam configuration.

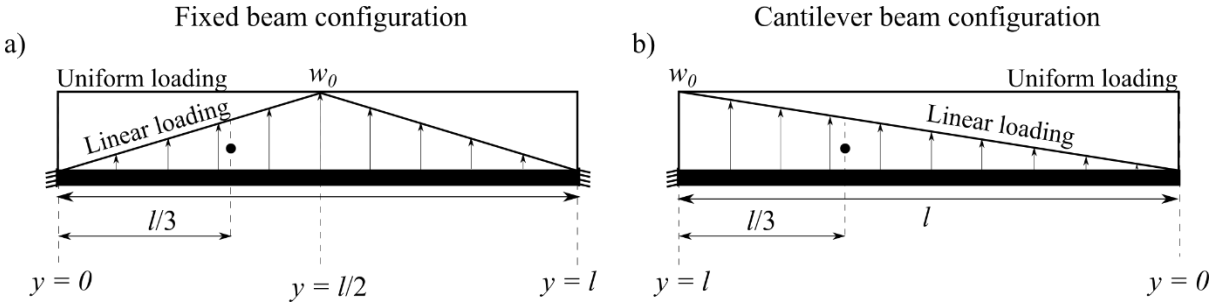

Figure 13 a) Fixed beam with uniform and linear loading and b) cantilever beam with unform and linear loading. The maximum distributed load is w_0. For the linear load case, the centroid of the equivalent load between $y = 0$ and $y = l/2$ in the fixed beam case and the centroid of the equivalent load between $y = 0$ and $y = l$ in the cantilever case are shown as black dots.

This project has received funding from the European Union's Horizon 2020 research and innovation programme under grant agreement No 851885. This output reflects the views only of the author(s), and the European Union cannot be held responsible for any use which may be made of the information contained therein.

Assuming two-dimensional flow (long span) and neglecting tip losses, the total force F on the fixed beam configuration can be computed as

$$F = L\cos\alpha + D\sin\alpha, \qquad \text{Eq. 5.2}$$

while the total force in the cantilever beam configuration is half of the force of Eq. 5.2, because figure 13b represents only half of the foil. The total force F can be distributed uniformly along the span of the hydrofoils by dividing the total force by the length of the hydrofoil, or in other words,

$$F = w_0 l, \qquad \text{Eq. 5.3}$$

where w_0 is the maximum distributed load and l is the length of the foil. Similarly, the local total force can be computed as

$$F_y = w_0 y, \qquad \text{Eq. 5.4}$$

where y is the local coordinate in the y-axis, where the force F_y is being computed, in a range between $0 \leq y \leq l$. The local origin in the y-axis of the beams ($y = 0$) is defined in figure 13.

For a linear loading the total force F applied to the beam is half of that of the load applied in uniform loading. This is because the area of a triangular shape is half of the rectangular area. As opposed to the previous case, the amplitude of the distributed load changes with y, an so we compute the expressions for the local distributed load (w_y) to compute the equivalent total force. For the fixed beam configuration

$$w_y = \frac{2w_0 y}{l} \qquad \text{Eq. 5.5}$$

in the range of $0 \leq y \leq l/2$ and for the cantilever configuration

$$w_y = \frac{w_0 y}{l} \qquad \text{Eq. 5.6}$$

in the range of $0 \leq y \leq l$. The total equivalent force in the fixed beam configuration can now be obtained by calculating the area of a triangle of base y and height w_y. So F_y for the fixed beam configuration is

$$F_y = \frac{w_0 y^2}{l} \qquad \text{Eq. 5.7}$$

in the range of $0 \leq y \leq l/2$ and for the cantilever configuration

$$F_y = \frac{w_0 y^2}{2l} \qquad \text{Eq. 5.8}$$

in the range of $0 \leq y \leq l$.

We can compute F_y from equations 5.4, 5.7 and 5.8 as a function of y, in the ranges of y specified above. The point of action of F_y is the centroid of the areas delimited by the different types of loading. For a triangle rectangle, the centroid is located at a 1/3rd distance from the right angle and its position is also a function of y.

As an example, the centroid of the equivalent load between $y = 0$ and $y = l/2$ in the fixed beam case and the centroid of the equivalent load between $y = 0$ and $y = l$ are shown as black dots in figures 13a and figure 13b, respectively.

This project has received funding from the European Union's Horizon 2020 research and innovation programme under grant agreement No 851885. This output reflects the views only of the author(s), and the European Union cannot be held responsible for any use which may be made of the information contained therein.

The equivalent force F_y is utilised in the free body diagrams to solve for the shear forces (V) and bending moments (M). The cantilever beam configuration is a determinate problem and V and M can be solved with the static equilibrium equations. The fixed beam configuration is an indeterminate problem, and the problem is not solved only with the static equilibrium equations. An additional equation is required. The additional equation is the general differential equation of the elastic curve:

$$EI\frac{d^2z}{dy^2} = M \qquad 5.9,$$

where M is the bending moment, E is the elastic modulus and I is the second moment of area. Equation 5.9 is integrated twice and by defining a set of boundary conditions the deflection on the beam (z) and the rest of the unknowns (V, M) can be solved. For the fixed beam, the boundary conditions are defined at the midpoint of the beam (maximum deflection) and at the origin of the beam (zero displacement). For the cantilever beam configuration, the boundary conditions are defined at the fixed end of the beam, with minimum deflection and zero displacement. The procedure can be applied to different types of loading, but the local distributed load equations (5.5 and 5.6) and the equivalent force equations (5.7 and 5.8) need to be recomputed.

Table 7 summarises the solutions for V, M and z for the two configurations (fixed beam, cantilever beam) subject to linear loading. The solutions for uniform loading can be found in structural mechanic text books. The equations were programmed in Python and results were validated with online solvers SkyCiv and ClearCalcs.

	Fixed beam	Cantilever beam
Shear forces (V)	$V = w_0 l\left(\frac{y}{l^2} - \frac{1}{4}\right)$	$V = w_0\left(\frac{y^2}{2l}\right)$
Bending moments (M)	$M = w_0\left(\frac{ly}{4} - \frac{y^3}{3l} - \frac{5l^2}{96}\right)$	$M = w_0\left(\frac{y^3}{6l}\right)$
Deflection (z)	$z = \left[\frac{1}{EI}\right]\left(\frac{w_0 l y^3}{24} - \frac{w_0 y^5}{60l} - \frac{5w_0 l^2 y^2}{192}\right)$	$z = \left[\frac{1}{EI}\right]\left(\frac{w_0 y^5}{120l} - \frac{w_0 l^3 y}{24} + \frac{w_0 l^4}{30}\right)$

Table 7. Shear forces (V), bending moments (M) and deflection (z) equations for a fixed beam and cantilever beam configurations subject to linear loading.

As an example of the fixed beam configuration, the V, M and z diagrams for uniform and linear loading are plotted in figure 14 versus the normalised span (S^*). The spans are normalised by the maximum length of the beam and the maximum length varies from 0 to 20 m. In the figure, the blue line represents the beam with the longest span and the dotted lines beams with decreasingly smaller span in steps of 1 m. A maximum distributed load of $w_0 = 1391.6$ N/m was used for this exercise, which corresponds to a distributed load computed with $C_L = 1.42$, $w = 1.4$ m/s and $c = 1$ m. Results show that for the fixed beam, maximum and minimum shear and maximum bending moments occur at both ends of the beams, whereas maximum deflection occurs in the middle of the beam.

This project has received funding from the European Union's Horizon 2020 research and innovation programme under grant agreement No 851885. This output reflects the views only of the author(s), and the European Union cannot be held responsible for any use which may be made of the information contained therein.

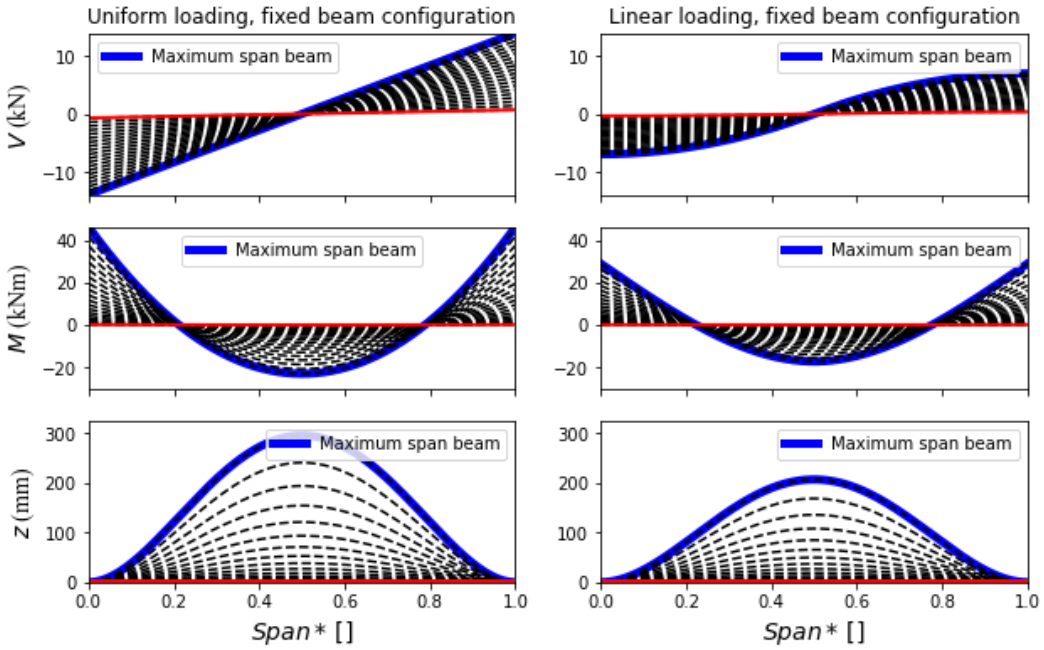

Figure 14 Shear (V), bending moments (M) and deflection (z) diagrams for uniform and linear loading for a fixed beam configuration. Spans vary from 0 (red line) to 20 meters (blue line).

For the cantilever configuration, the maximum shear and bending moments occur at the fixed end of the hydrofoils, whereas maximum deflection occurs at the free end. Figure 15 shows the results using for the cantilever beam using also $w_0 = 1391.6$ N/m. The free end is on the left of the subfigures. Flapwise deflections as the ones observed in the bottom row of figure 15 could induce spanwise flow in the blades challenging the assumption of two dimensional flow (Adcock, et al. 2020). Hence, the effect of these deflections on spanwise flow need to be considered in future load assessments.

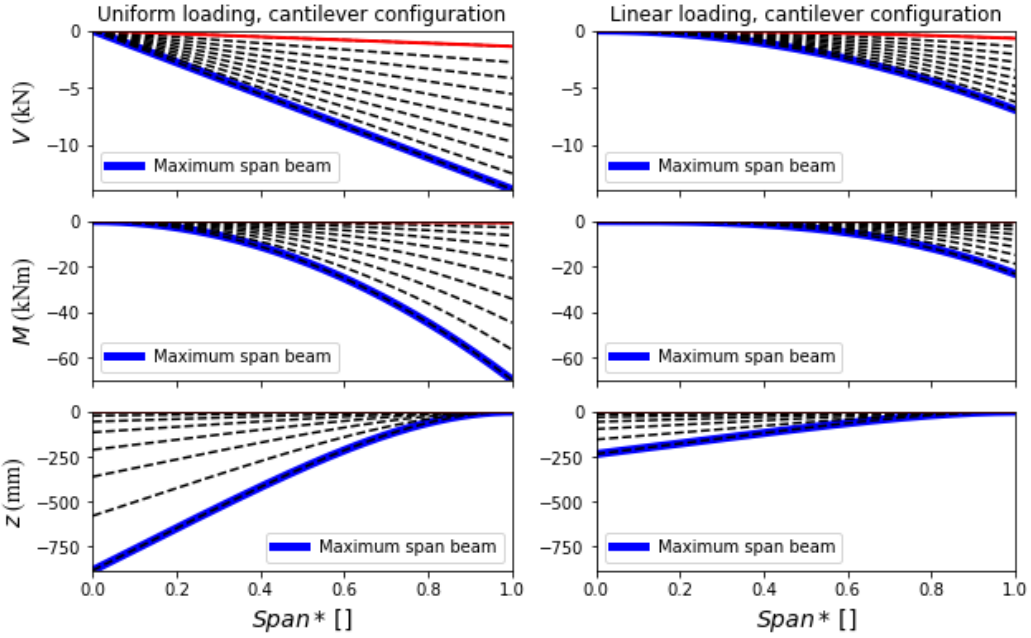

Figure 15 Shear (V), bending moments (M) and deflection (z) diagrams for uniform and linear loading for a cantilever beam configuration. Spans vary from 0 (red line) to 20 meters (blue line).

This project has received funding from the European Union's Horizon 2020 research and innovation programme under grant agreement No 851885. This output reflects the views only of the author(s), and the European Union cannot be held responsible for any use which may be made of the information contained therein.

5.3.1 Maximum bending moments

In this subsection, the maximum bending moments and bending stresses are computed for uniform and linear loading for the two types of tested configurations (fixed beam and cantilever beam). The maximum bending moments are shown in figure 16a and figure 16b for spans varying between 0 to 60 meters. A maximum span of 60 meters is considered because Siegel's cyclorotor is sized to this length (Siegel 2019). In his study, he considered a rotor radius of 5 meters. Here we consider radiuses in the range of 1 to 4 mts.

Figure 16 shows that the maximum bending moments increase with the span and with the chord length. The slope of the curves is steeper in uniform loading. It is also observed that when subject to uniform loading, the cantilever configuration experiences higher moments than the fixed beam configuration. The trend reverses when linear loading is applied.

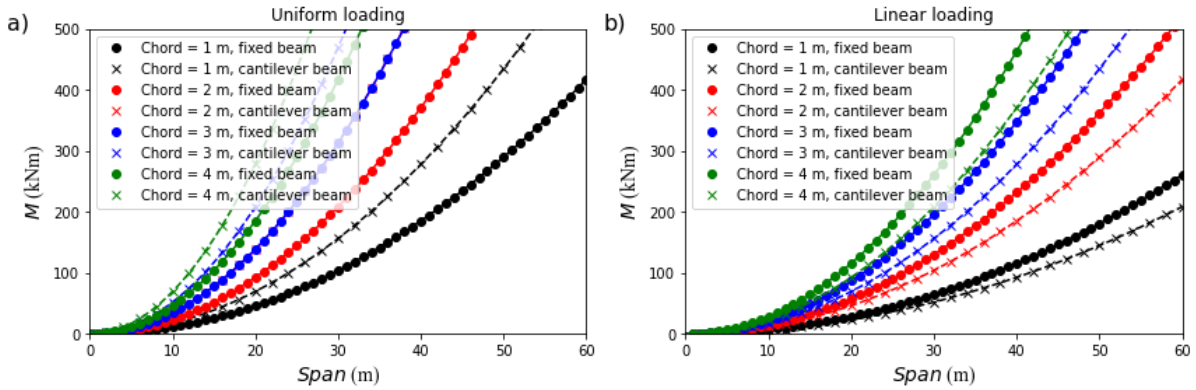

Figure 16 a) Uniform and b) linear loading maximum bending moments M versus span for the fixed beam (dots) and cantilever (crosses) configurations. Four different chord lengths are plotted: 1 m (black), 2 m (red), 3 m (blue) and 4 m (green).

5.3.2 Maximum bending stresses

Figure 17a and figure 17b show the maximum bending stresses subject to uniform and to linear loading. In the figures, the yellow dotted line is the threshold for the allowable stress level and the red dotted line is the threshold for the yield stress of offshore structural steel. Results show that stresses in the foils decrease with increasing chord length and increase with increasing span length.

We note that for uniform loading, a fixed beam configuration is preferred over a cantilever beam configuration due to lower stresses on the former one. The contrary is preferred if linear loading is applied. Depending on the type of loading and the chord length, the foils could be sized between 20 to 35 meters to remain below the allowable stress level threshold. Our analysis shows that a 60 meters span device could operate in close proximity to the yield stress of offshore structural steel and therefore we recommend a more conservative approach in fixed and cantilever beams configurations.

This project has received funding from the European Union's Horizon 2020 research and innovation programme under grant agreement No 851885. This output reflects the views only of the author(s), and the European Union cannot be held responsible for any use which may be made of the information contained therein.

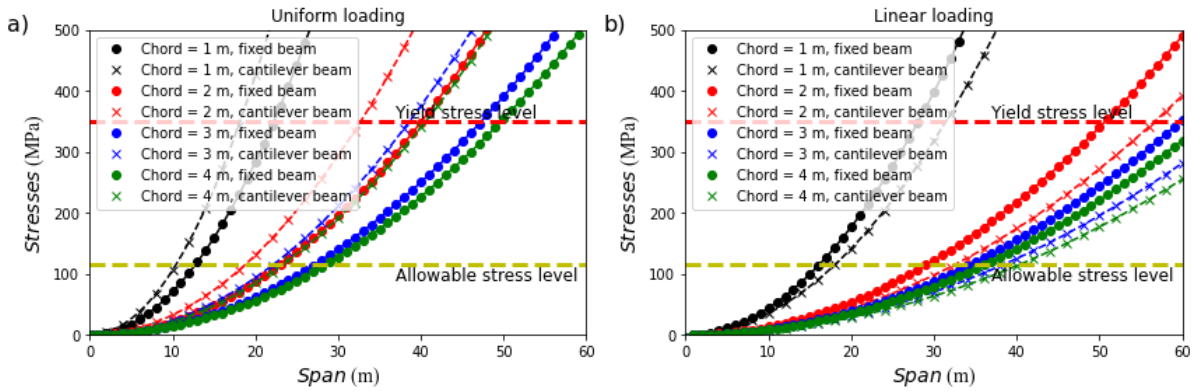

Figure 17 a) Uniform and b) linear loading maximum bending stresses versus span for the fixed beam (dots) and cantilever (crosses) configurations. Four different chord lengths are plotted: 1 m (black), 2 m (red), 3 m (blue) and 4 m (green).

5.4 SPOKES AND DISKS ANALYSIS

In this section we analyse the substructures connecting the hydrofoils to the hub or for hubless configurations, to the PTO. The classification diagram of figure 3 shows that the connection can be either a spoke or a disc. The forces on these substructures act axially (see figure 8a) either in tension or compression. We conduct the analysis for axial tension, considering that steel is equally strong in tension and compression.

5.4.1 Spokes

The stresses of a bar under axial tension are given by

$$\sigma = \frac{F}{A}, \qquad \text{Eq. 5.10}$$

where F is the applied load and A is the cross-sectional area before loading (Young and Budynas 2002). The deformation of a bar under axial tension can be computed with

$$\delta = \frac{Fl}{AE}, \qquad \text{Eq. 5.11}$$

where l is the length of the bar and E is the modulus of elasticity.

Consider the spoke diagram of figure 18. In the figure the thickness is th, the width is wd, the original length is l and F is the total axial force applied to the spoke.

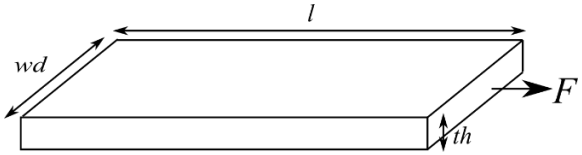

Figure 18 Axial load F acting on spoke of dimension $l \times wd \times th$.

This project has received funding from the European Union's Horizon 2020 research and innovation programme under grant agreement No 851885. This output reflects the views only of the author(s), and the European Union cannot be held responsible for any use which may be made of the information contained therein.

The total force F can be computed with equations 5.2. For a cantilever beam configuration (singly supported foil), F will act only on one spoke. For a fixed beam configuration F will be shared equally between two spokes. We can compute σ and δ for the spoke for these two possible scenarios, by utilising equations 5.10 and 5.11.

From figure 17a, we choose a foil with $b =$ 30 m and $c = 4$ m. We recall that $C_L = 1.42$, and $C_D =$ 0.0141 at $\alpha = 14^{\circ}$ and that ρ = 1000 kg/m^3. We consider $w = 1.4$ m/s. Using equation 5.2 the total load acting in a single spoke is $F = 171$ kN. The load is halved for the case of doubly supported foil. Axial stresses on the spoke are plotted in figure 18a versus the width to thickness ratio (wd/th). Four thicknesses (th) are utilised ($th = 10, 25, 50, 100$ mm) and one case is validated with software Abaqus (black cross marker).

Results of figure 19a show that two spokes undergo less axial stresses than a single spoke. This is most significant when the thickness of the spoke is small ($th < 10$ mm). When the thickness increases ($th \geq 25$ mm) the performance is not significantly changed because the stresses start converging towards very low values. The figure can be utilised to ensure that the wd/th ratio chosen for the design will remain below the allowable stress level.

The deflections of the spokes versus range of stresses measured in figure 19a are shown in figure 19b. Here we study how the thickness and the length of the spokes affect the deformation (δ). We consider lengths of $l = 250, 500, 750$ and 1000 mm, which would correspond to the rotor radius (r). We study two different thicknesses ($th = 10$ mm and $th = 25$ mm). The elastic modulus for steel is $E =$ 210000 MPa. Most of the tested cases have a deformation below 1 mm. It is observed that the longer and thinner, the more the spoke will deform. The required level of deformation needs to be considered in order to size the dimensions of the spoke. However they are resilient structures to tension (and compression) as shown in figure 19a.

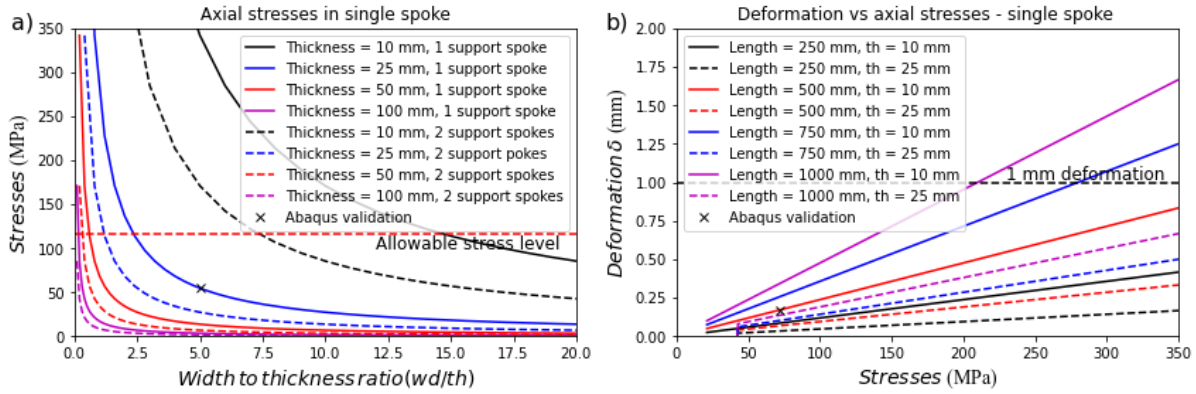

Figure 19 a) Axial stresses versus width to thickness ratio on different thickness spokes for singly supported foil and doubly supported foil, b) deformations versus stresses for different spoke lengths and thicknesses.

The outputs of equations 5.10 and 5.11 were validated with Abaqus, and the two dimensional finite element analysis setup is shown in figure 20. In the setup, an axial force is applied on one side of a two dimensional bar, which is fixed at its opposite boundary. The stresses and deflections are measured and compared with analytical results.

This project has received funding from the European Union's Horizon 2020 research and innovation programme under grant agreement No 851885. This output reflects the views only of the author(s), and the European Union cannot be held responsible for any use which may be made of the information contained therein.

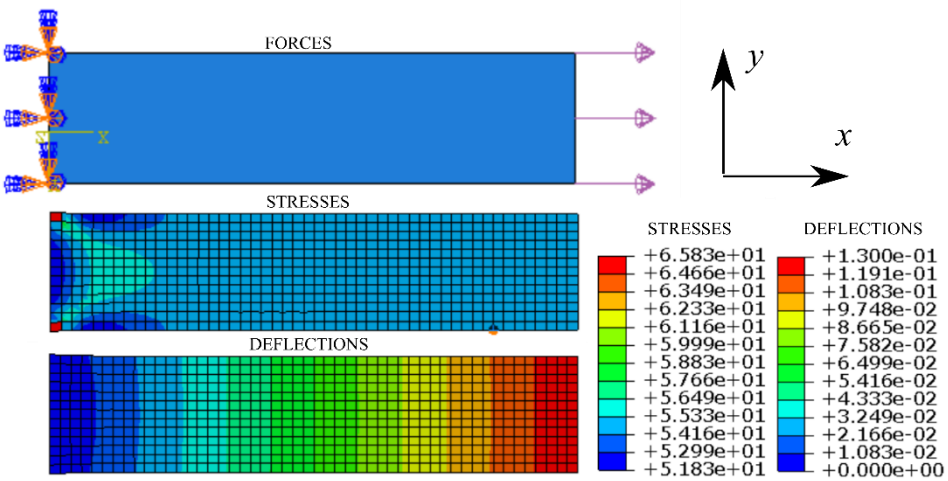

Figure 20 Finite element analysis of spoke, where load F is applied axially to one end of spoke and opposite end is constraint in all directions. The figure shows the forces, stress levels and deformation contours (top to bottom) showing uniform stresses along the spoke and maximum deflection at the tip of the spoke.

5.4.2 Discs

The support structure for the foil can be a disc. Applying an axial load to a disc through finite element analysis provides different results depending on how the force is applied to the disc (point load or distributed). Therefore, for this part of the analysis, only a qualitative analysis is performed on the disc. The load is applied in a distributed manner as depicted in figure 21. Our analysis shows that the stress levels are expected to remain in the same order of magnitude as those predicted for the spokes. The maximum stresses will be located towards the outer edge of the discs. In contrast, the deflection levels of the disc are smaller than those of the spoke. This is expected since more material is expected to deform less subject to the same load.

There does not seem to be a significant structural advantage on the use of discs with respect to the spokes. It is also expected that the obstruction to the flow is smaller with the spokes and the manufacturing costs will also be reduced. Hence, this preliminary analysis suggest that spokes should be preferred over discs as support structures for the hydrofoils.

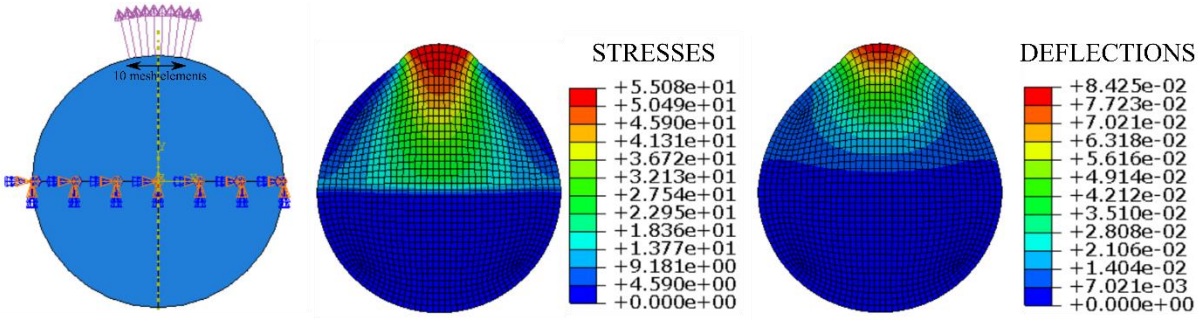

Figure 21 Finite element analysis of disc, where load F is applied axially to one end of the disc and the middle section of the disc is constraint in all directions. The figure shows the forces, stress levels and deformation contours (left to right) showing the highest stresses and deformations towards the edge of the disc where the force is applied.

This project has received funding from the European Union's Horizon 2020 research and innovation programme under grant agreement No 851885. This output reflects the views only of the author(s), and the European Union cannot be held responsible for any use which may be made of the information contained therein.

5.5 SUPPORT STRUCTURE ANALYSIS

We consider a maximum lift coefficient on hydrofoil 1 of $C_{L1} = 1.4$ and maximum inflow velocity of $U_1 = 1.42$ m/s. For hydrofoil 2 we consider maximum values of $C_{L2} = 1.4$ and $U_2 = 1.3$ m/s. These values were obtained from the simulation performed to generate figure 9. We note that maximum C_L for both hydrofoils (NACA 0012) occurs at $\alpha = 14^{\circ}$.

We consider a bottom fixed structure, as the one shown in figure 22. The reaction forces due to the lift and drag forces on hydrofoil 1 and hydrofoil 2 are $R_1$and R_2. As show in the figure, both reaction forces act in the same direction. The moment (M) is caused by the tangential forces F_{tan1} and F_{tan2} and is computed as

$$M = [F_{tan1} + F_{tan2}]\, r,$$

where r is the radius of the hub. From figure 8a, the tangential forces can be computed as

$$F_{tan1} = \frac{1\rho U_1^2 bc}{2}[C_{L1}\sin\alpha - C_{D1}\cos\alpha] \quad \text{and} \quad F_{tan2} = \frac{1\rho U_2^2 bc}{2}[C_{L2}\sin\alpha - C_{D2}\cos\alpha]$$

where ρ is the density of the fluid, b is the span of the hydrofoil, c is the chord length and α is the angle of attack of the hydrofoils. In this case, $\alpha = 14^{\circ}$.

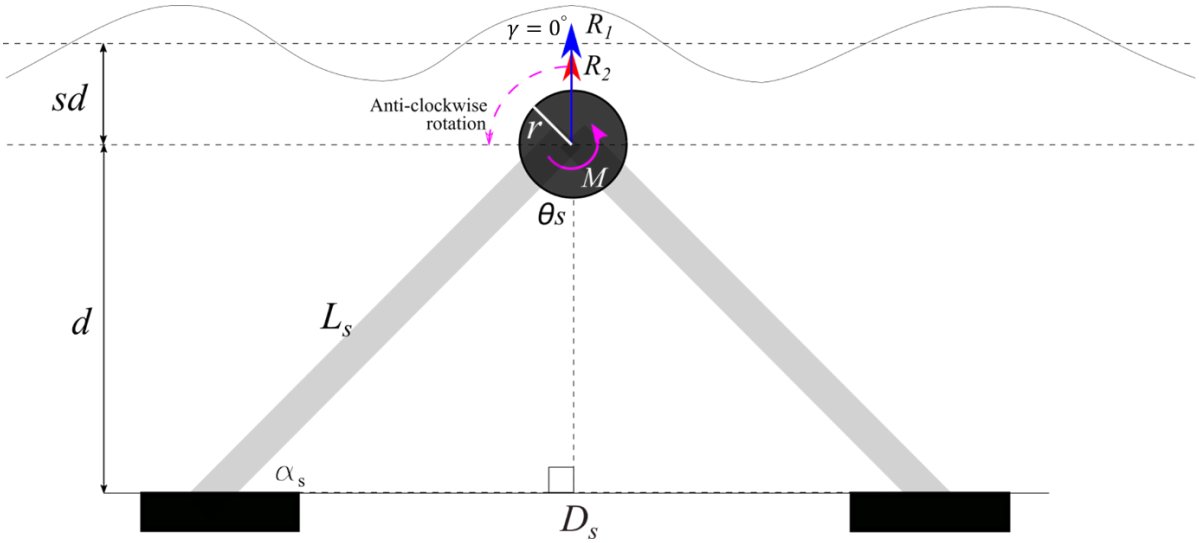

Figure 22 Bottom fixed structure with reactions forces (R_1, R_2) and moment (M). In the figure, the submerged depth is sd, the height of structure is d, the length of the support beam is L_s, the spacing between the two anchoring points is D_s, and the non-rectangular angles inside of the structure are α_s and θ_s.

5.5.1 Shear forces and bending moments envelopes

As an example, we first show how the shear and bending moment diagrams vary as the reaction forces rotate anti-clockwise around the hub from $\gamma = 0^{\circ}$ to $\gamma = 270^{\circ}$, where $\gamma = 0^{\circ}$ is the azimuthal direction pointing towards the vertical and positive axis (as shown in figure 22). We consider two fixed supports and utilise online solver SkyCiv to solve the diagrams. The online solver was validated for determinate and indeterminate frame structures problems. We consider a height for the structure of $d = 30$ m and a spacing between the two anchoring points of D_s = 60 m, as in Siegel (2019).

This project has received funding from the European Union's Horizon 2020 research and innovation programme under grant agreement No 851885. This output reflects the views only of the author(s), and the European Union cannot be held responsible for any use which may be made of the information contained therein.

Results are shown in figure 23, for $\gamma = 0^{\circ}$, 90°, 180° and 270° from top to bottom. It can be observed that the shear force diagrams are asymmetrical at $\gamma = 0^{\circ}$ and $\gamma = 180^{\circ}$, and symmetrical at $\gamma = 90^{\circ}$ and $\gamma = 270^{\circ}$.The maximum bending moments occur in the cases where the shear forces are asymmetrical, i.e. $\gamma = 0^{\circ}$ and $\gamma = 180^{\circ}$.

REACTION FORCES **SHEAR FORCES** **BENDING MOMENTS**

$\gamma = 0^{\circ}$, FIXED SUPPORTS

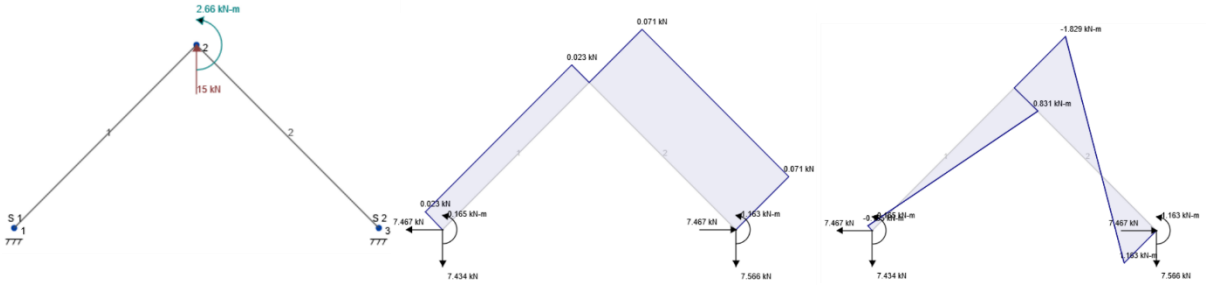

$\gamma = 90^{\circ}$, FIXED SUPPORTS

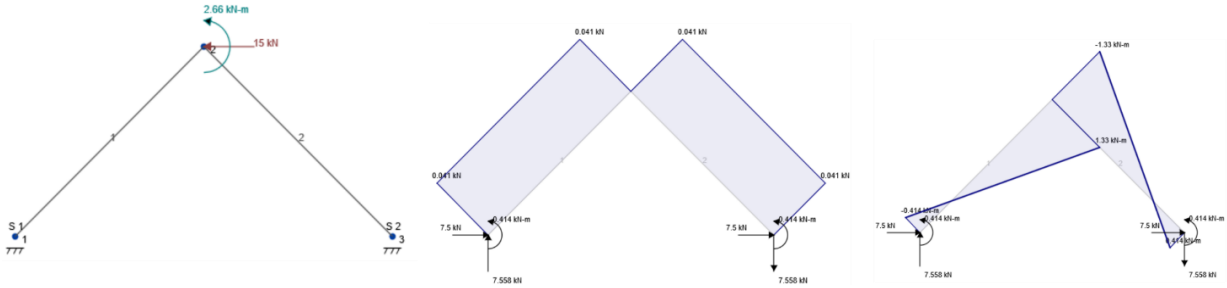

$\gamma = 180^{\circ}$, FIXED SUPPORTS

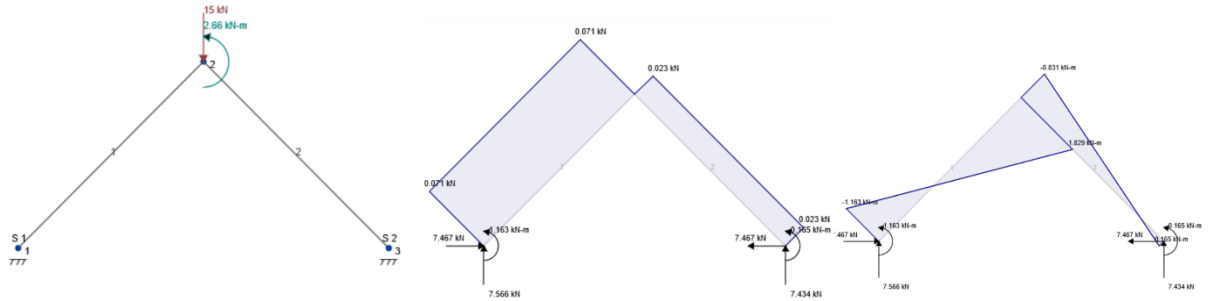

$\gamma = 270^{\circ}$, FIXED SUPPORTS

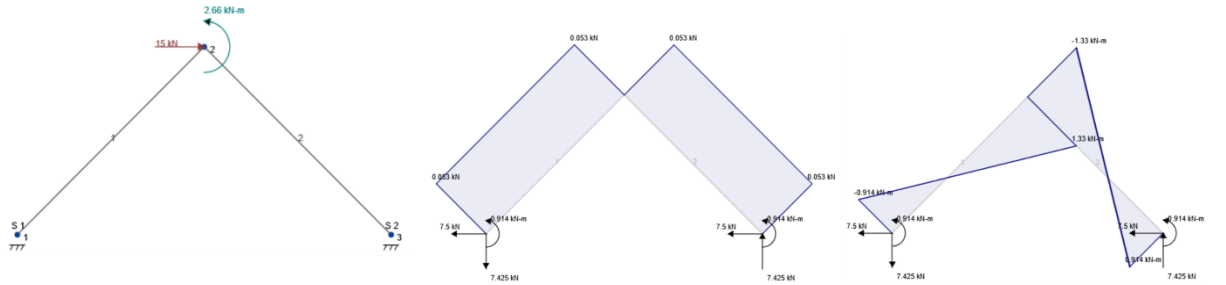

Figure 23 Reaction forces, shear forces and bending moment diagrams for support structure computed with SkyCiv, at $\gamma = 0^{\circ}, \gamma = 90^{\circ}, \gamma = 180^{\circ}$ and $\gamma = 270^{\circ}$.

This project has received funding from the European Union's Horizon 2020 research and innovation programme under grant agreement No 851885. This output reflects the views only of the author(s), and the European Union cannot be held responsible for any use which may be made of the information contained therein.

5.5.2 Maximum and minimum bending moments and bending stresses at different γ

Considering two fixed supports, we compute the maximum bending moments and bending stresses for the four azimuthal positions $\gamma = 0^{\circ}, 90^{\circ}, 180^{\circ}$ and 270°. We vary the span of the hydrofoils from 0 to 60 meters. We consider $c = 1$ m, $d = 30$ m, D_s = 60 m. The reaction forces R_1 and R_2 are computed with $C_{L1} = 1.4$, $C_{L2} = 1.4$, $U_1 = 1.4$ m/s, $U_2 = 1.3$ m/s, $C_{D1} = 0.0157$ and $C_{D2} = 0.0157$. The submergence is -3 meters, as in section 4. Maximum and minimum bending moments occur at $\gamma = 180^{\circ}$ and $\gamma = 0^{\circ}$, respectively, as shown in figure 24a. Figure 24b shows that the maximum and minimum bending stresses remain away from the allowable stress levels, and so the support structure should be less prompt to structural damage than the hydrofoils. For this analysis we considered hollow square section for the support structure of 0.25 m x 0.25 m.

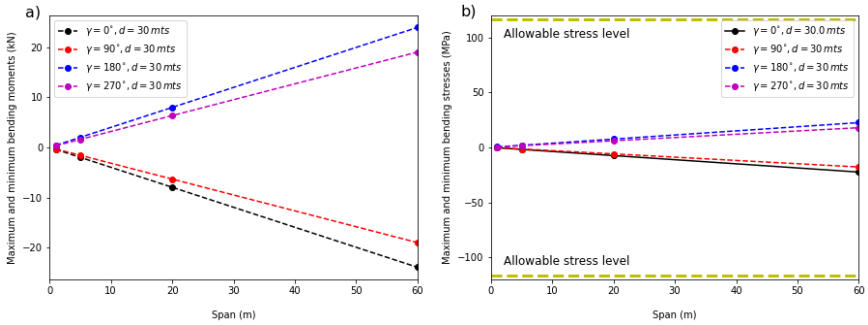

Figure 24 a) Maximum bending moments and b) maximum and minimum bending stresses in support structure for different spans at $\gamma = 0^{\circ}, \gamma = 90^{\circ}, \gamma = 180^{\circ}$ and $\gamma = 270^{\circ}$, and $d = 30$ m.

5.5.3 Effect of height of the structure and of rotor radius in bending stresses

We explore the effect of the height of the structure and the radius of the rotor. First, we zoom in at figure 24b and we take the baseline of $\gamma = 0^{\circ}$ and a height $d = 30$ m (black dotted line). We vary the height to $d = 15$ m and $d = 45$ m. Results are shown in figure 25a. It is shown that the shorter the structure the higher the maximum bending moments. Hence tall structures are preferred structurally. Secondly, we keep the height of the structure constant ($d = 30$ m) and decrease the rotor radius from $r = 1$ m to $r = 0.75$ m and $r = 0.5$ m. Figure 25b shows that a smaller rotor will generate smaller bending moments on the structure, however this will compromise the torque and therefore might not be the preferred option. It is observed that a rotor radius of 1 m is below the allowable stress level.

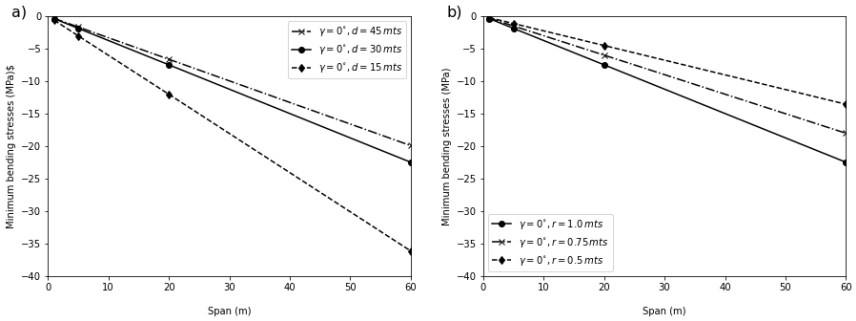

Figure 25 a) Minimum bending stresses in support structure at $\gamma = 0^{\circ}$ at different heights ($d = 15, 30$ and 45 m) and b) minimum bending stresses in support structure at $\gamma = 0^{\circ}$ for different rotor radius ($r = 1, 0.75$ and 0.5 m) computed with different hydrofoil spans.

This project has received funding from the European Union's Horizon 2020 research and innovation programme under grant agreement No 851885. This output reflects the views only of the author(s), and the European Union cannot be held responsible for any use which may be made of the information contained therein.

6 SUMMARY OF METHODOLOGY

The steps to carry out the structural analysis of the LiftWEC rotor are summarised in the block diagram of figure 26. The method is flexible and can incorporate more advanced hydrodynamic models. Future work will include investigating the flapwise deformation effects in the load distribution of the hydrofoils.

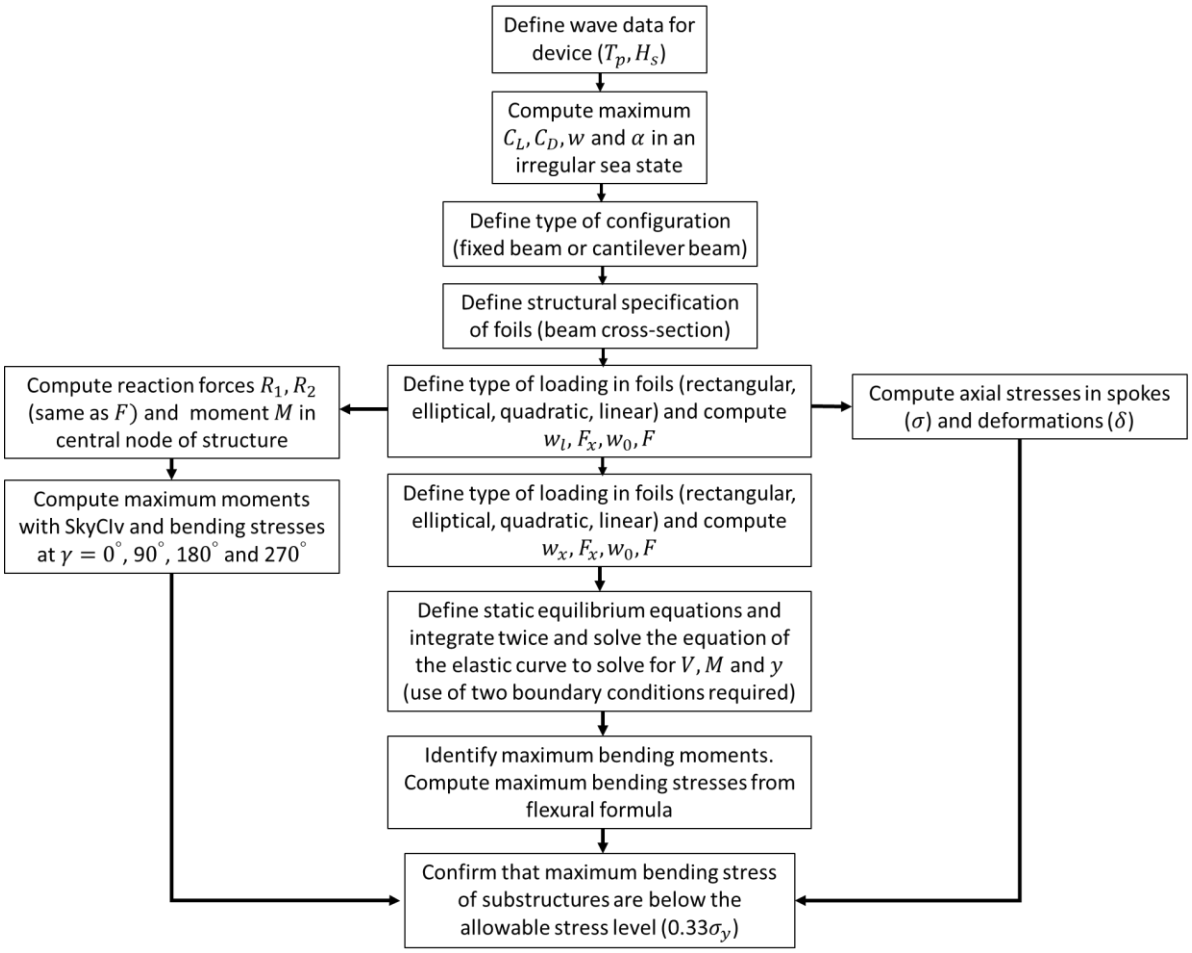

Figure 26 Summary of methodology for the structural assessment introduced in this deliverable.

This project has received funding from the European Union's Horizon 2020 research and innovation programme under grant agreement No 851885. This output reflects the views only of the author(s), and the European Union cannot be held responsible for any use which may be made of the information contained therein.

7 CONCLUSIONS

This work presents a global structural assessment methodology for the LiftWEC device. Loads on LiftWEC are maximum during operating conditions and hence this is considered to be the ultimate limit state (ULS). However, the methodology is flexible to test different operating conditions, by varying the wave data and rotor operating conditions (see Appendix 2).

An irregular sea state is utilised to predict the maximum C_L, C_D, w and α that the rotor can experience in the design state. These maximum values are used to compute the equivalent total loads (F) and the equivalent local loads (F_y) over different span hydrofoils. The hydrofoils are modelled as beams. A type of loading is specified over the beam. A free body diagram sets out the static equilibrium equations, which are solved directly for determinate beams (cantilever configuration). For indeterminate beams (fixed beams), the static equilibrium equations are solved with and additional equation (the equation of the elastic curve).

Shear forces, bending moments and deflections on the beams are solved for different span hydrofoils and maximum bending moments are detected. Subsequently, they are used to compute the maximum bending stresses on the substructure. The equivalent loads F are used to compute the axial stresses and deformations on the spokes. And F and the tangential forces are used to compute the maximum bending moments and bending stresses of a bottom fixed frame structure. The results are checked for an anticlockwise rotation of the reaction forces around the central hub of the structure.

Finally, the maximum bending stresses of the substructures (hydrofoils, spokes and support structure) are compared against the allowable stress level threshold. It is found that among all of the substructures, the hydrofoils are the ones exposed to higher bending moments. For large aspect ratios hydrofoils ($AR \geq 3$), the flow on the foil will tend to be two dimensional and uniform loading is expected. Results show that for uniform loading a fixed beam configuration is preferred over a cantilever beam configuration. It is also shown that the recommend span for a large-scale device, of a 4 m chord length, lies in the range of 30 to 40 m. This contrasts the dimensions of CycWEC, which is sized to 60 m for a chord length of 5 m.

8 REFERENCES

Adcock, Thomas A. A., Scott Draper, Richard H. J. Willden, and Christopher R. Vogel. 2020. “The Fluid Mechanics of Tidal Stream Energy Conversion.” *Annu. Rev. Fluid Mech.* 53: 287-310.

Airy, G. B. 1845. “On tides and waves.” *Encyclopaedia Metropolitana* 5 (London: B. Fellowes): 241-396.

Billingham, J, J. V. Sharp, J. Spurrier, and P.J. Kilgallon. 2003. *Review of the performance of high strength steels used offshore. Research Report 105.* Cranfield University for the Health and Safety Executive 2003 .

Bouet, Lola, and Rémy Pascal. 2020. “Deliverable D3.1 - Uncoupled Model of LiftWEC for preliminary concept assessment.” *LiftWEC.*

This project has received funding from the European Union’s Horizon 2020 research and innovation programme under grant agreement No 851885. This output reflects the views only of the author(s), and the European Union cannot be held responsible for any use which may be made of the information contained therein.

Cantwell, B. J. 2019. *AA200_Ch_12_Wings_of_Finite_Span_Cantwell.pdf.* 25 03. Accessed 11 02, 2020. https://web.stanford.edu/~cantwell/AA200_Course_Material.

Cornet, Andrew M. 2008. "A global wave energy resource assessment." *The Eighteenth International Offshore and Polar Engineering Conference.* Vancouver, Canada: International Society of Offshore and Polar Engineers.

DeVoria, A. C., and K. Mohseni. 2017. "On the mechanism of high-incidence lift generation for steadily translating low-aspect-ratio wings." *Journal of Fluid Mechanics* 110-126.

DNV-GL. 2017. "Certification of Wave Energy Converters and Arrays (draft)." *DNVGL-SE-0120* (DNV GL).

Emarkov, Andrei. 2020. "LW-WP01-AE-R01-7x0 The Control Problem for LiftWEC." *Consortium Report* 1-12.

Guillou, Nicolas, and Georges Chapalain. 2018. "Annual and seasonal variabilities in the performances of wave." *Energy* 165 (Part B, 15): 812-823.

Jeans, T.I., C. Fagley, S.G. Siegel, and J. Seidel. 2013. "Irregular deep ocean wave energy attenuation using a cycloidal wave energy converter." *International Journal of Marine Energy* 16-32.

Pascal, Rémy, Nicolas Clave, and Matt Folley. 2020. "Deliverable D2.2 - Identification of evaluation criteria." *LiftWEC* (LiftWEC).

Prandtl, L. 1923. "Applications of modern hydrodynamics to aeronautics." *NACA Technical Report. No. 116.*

Sheldahl, Robert E., and Paul C. Klimas. 1981. "Aerodynamic Characteristics of Seven Symmetrical Airfoil Sections Through 180-Degree Angle of Attack for Use in Aerodynamic Analysis of Vertical Axis Wind Turbines." *Sandia National Laboratories Energy Report.*

Siegel, Stefan. 2012. "Cycloidal Wave Energy Converter. Atargis Energy Corporation, DUNS #962384686." *Final Scientific Report.*

Siegel, Stefan G. 2019. "Numerical benchmarking study of a Cycloidal Wave Energy Converter." *Renewable Energy* 134: 390-405.

Sierra, Joan Pau, Adam White, Cesar Mosso, and Marc Mestres. 2017. "Assessment of the intra-annual and inter-annual variability of the variability of the wave energy resource in the Bay of Biscay (France)." *Energy* 853-868.

SteelConstruction.info. n.d. *Steel for life. Interactive 'Blue book'.* Accessed 11 4, 2020. https://www.steelforlifebluebook.co.uk/.

WES, The University of Edinburgh, ESC, WavEC, Tecnalia. 2020. *DTOceanPlus Deliverable D4.2 Stage Gate tool – Alpha version.* Edinburgh: DTOceanPlus.

Young, Warren C., and Richard G. Budynas. 2002. *Roark's Formulas for Stress and Strain.* 7th Edition. New York: McGraw-Hill.

This project has received funding from the European Union's Horizon 2020 research and innovation programme under grant agreement No 851885. This output reflects the views only of the author(s), and the European Union cannot be held responsible for any use which may be made of the information contained therein.

9 APPENDIX 1

This appendix shows the classification of commonalities performed for the seventeen prototypes. This classification helped in organising the protypes and elaborate the tree diagrams of section 2.

The columns of the table in the appendix are: Device type, type of mooring, central shaft, spokes, PTO, reaction source, hydrofoil reaction source and endplates.

Device type	Type of mooring	Central shaft	Spokes	PTO	Reaction source	H. reaction source	Endplates
Jack-up CycWEC	Relescopic hinged jack-up struts	Yes	2 (Inside nacelle)	Shaft generator	Seabed	Seabed	Disk
LiftWEC proposal configuration	Jackup strut supports	Yes	2	Shaft generator	Seabed	Seabed	None
Hydrofoil mounted turbine PTO	Triangular strcutre & micropiles	Yes	1	MINESTO type	Seabed	Radial struts	None
Adaptable - reconfigurable WEC	Variable depth, telescopic struts	Yes	Telescopic, 1	Shaft generator	Seabed	Radial struts	None
Twin-moored buoyant structure	Front V mooring and rear Y mooring	Yes	None	MINESTO type	Not spec	Mooring to seabed	Disk
Spar buoy with phase free rotor	Spar-slack single point moored platform	Yes	None	Shaft generator	Inertia	Rotor linked to gen	Disk
Parabolic with flaps	Stiff tubes single point V-mooring	Yes	NA	Shaft generator	Seabed	NA	NA
Phase-locked contra-rotating	Monopile - as in tidal energy - 2 rotors	Yes	2	Shaft generator	Seabed	Contra rotating rotors	None
Struts based single rotor	Jack-up strut supports	No	None	DD Generator	Seabed	Generator structure	Disk
Tethered mono-hydrofoil	Syntetic lines for mooring lines	No	NA	MINESTO type	Seabed	Surrounding water	None
Direct hydrofoil rotor PTO	Fixed or floating	No	2	MINESTO type	Seabed/floater	Radial struts	None
Slack moored LiftWEC semisub	Syntetic lines for mooring lines	Yes	2	Shaft generator	Slacked moored	Floating semisub str	None
Hydraulic PTO	Sea mounted	Yes	2	Hydraulic	Seabed/floater	Struts	None
Hubless wing	Seabed	No	None	MINESTO type	Seabed	Seabed	Winglets
Radius Control Focused Config	Support structure	Yes	2	Shaft generator	Seabed	Seabed	None
Planetary Gear End Plates	Fixed mooring and v-shape tubes	No	None	Planetary gear	Seabed	Disk	Disk
Single Strut Hydrofoil	Taut mooring system	Yes	1	MINESTO type	Seabed	Radial strut	Winglets

10 APPENDIX 2

The rotor properties and operational parameters were chosen as follows:

Parameter	Measurement
Rotor radius (r)	1 m
Submergence (sd) (measured to centre of rotor)	-3 m
Chord length (c)	1 m
Significant wave height (H_s)	4 m
Peak period (T_p)	10 s
Rotational velocity (u)	0.6283 m/s
Phase	90 deg

This project has received funding from the European Union's Horizon 2020 research and innovation programme under grant agreement No 851885. This output reflects the views only of the author(s), and the European Union cannot be held responsible for any use which may be made of the information contained therein.